Technical Note

Verification of ASCE 7-16 Pressure Coefficients and Database-Assisted Design of Purlins and Girts Accounting for Wind Directionality

Dat Duthinh, M.ASCE[1]; and Emil Simiu, F.ASCE[2]

Abstract: For the database-assisted design (DAD) of low-rise building purlins and girts, a method is proposed that explicitly accounts for wind directionality by using directional wind tunnel measurements, directional wind speed data, and publicly available software. The method consists of four steps: (1) assignment of wind loads induced by a unit directional wind speed on purlins and girts from pressure taps and their tributary areas; (2) development of bending moment and shear force influence coefficients for line loads on purlins and girts; (3) multiplication of loads from step 1 by influence coefficients from step 2 and estimation of the peak bending moments and shear forces thus obtained; and (4) use of nonparametric statistics to calculate peak moments and shear forces with a specified mean recurrence interval for various building orientations and accounting for wind directionality. For one example of wind effects on purlins, (1) comparison of the Envelope Method in ASCE 7-16 (taken as 100%) with the most demanding aerodynamic case from wind tunnel tests shows differences ranging between +10% and −25%; and (2) comparison of the ASCE 7-16 method accounting for the wind directionality factor K_d with directional wind loads using nonparametric statistical methods shows differences ranging between +21% and −25%. The unconservatism (+) of ASCE 7-16 is thus worse after K_d is applied. The proposed method is based on the rigorous DAD approach, accounts explicitly for the actual directional wind loading, entails no onerous computational requirements, and typically results in more economical designs while assuring risk-consistent safety. **DOI: 10.1061/(ASCE)ST.1943-541X.0002543.** © *2020 American Society of Civil Engineers.*

Author keywords: Bending moment; Database-assisted design; Directional effects; Girts; Influence coefficients; Purlins; Shear force; Time series; Wind pressure; Wind tunnel tests.

Introduction

Current design of low-rise buildings relies on wind pressure coefficients, nondirectional wind speed maps, and a wind directionality factor $K_d = 0.85$ specified by ASCE 7-16 (ASCE 2017) or its predecessors. "This factor accounts for two facts: (1) the reduced probability of maximum winds coming from any given direction, and (2) the reduced probability of the maximum pressure coefficient occurring for any given wind direction" [ASCE 7-16 (ASCE 2017, §C26.6)]. As computational capabilities improve, and publicly available databases of wind tunnel tests and directional wind speeds increase their scope, it is becoming attractive to design structures for wind by taking explicit account of wind direction, thus bypassing simplified design charts and tables and a wind direction reduction factor. This paper presents a method that does so for the design of the roof purlins of low-rise buildings and is also directly applicable, with no modification, to wall girts. The method is illustrated by an example in which moments and shear forces are determined for the roof purlins of Building 7 tested in open country exposure [data set jp1 of the NIST-UWO database, NIST (2004a), which also contains data for suburban exposure]. The building was modeled at a length scale of 1:100, and data were collected for 100 s at 500 Hz. Building 7 is 12 m (40 ft) wide, 19 m (62.5 ft) long, 12 m high (40 ft, eave height), and has a roof slope of 1:12 (4.8°). It was tested for wind directions θ_a ranging from 0° to 90° and 270° to 360° every 5°. Due to building symmetry, and for similar terrain exposure in all directions, only half of all possible wind directions needed to be investigated. The paper starts with a review of the literature, followed by the exposition of the method, results, and conclusions.

Literature Review

Interest in database-assisted design stems from advances in pressure measurement and computer technology that allow simultaneous recording and rapid processing of many more pressure taps (on the order of hundreds) than was possible a few decades ago. Furthermore, wind tunnel test measurements have become publicly available for considerably more building geometries. The most referenced publicly available sources of data are the NIST (2004a, b) database, which covers tests conducted at the University of Western Ontario (UWO) (Ho et al. 2003a, b), and the Tokyo Polytechnic Institute (TPU) (Tamura 2012) database. The Supplemental Data summarizes the dimensions of the test models available in these two databases, which include rectangular buildings of various dimensions and roof configurations.

Jayasinghe et al. (2018) investigated the distribution of wind loads onto a roof system consisting of metal cladding, battens, and trusses. They tested 16 roof panels supported by five trusses 900 mm (35 in.) apart and five battens spaced between 600 mm (24 in.) and 750 mm (30 in.), under point loads, and measured the loads transferred by the battens to the trusses. They concluded that the conventional (in Australia) method of assigning pressures

[1]Research Structural Engineer, Engineering Laboratory, National Institute of Standards and Technology, Gaithersburg, MD 20899 (corresponding author). Email: dduthinh@nist.gov

[2]NIST Fellow, Engineering Laboratory, National Institute of Standards and Technology, Gaithersburg, MD 20899. Email: emil.simiu@nist.gov

Note. This manuscript was submitted on August 30, 2018; approved on August 2, 2019; published online on January 8, 2020. Discussion period open until June 8, 2020; separate discussions must be submitted for individual papers. This technical note is part of the ***Journal of Structural Engineering***, © ASCE, ISSN 0733-9445.

measured from roof taps to supporting structural members could be improved by structural analysis.

Shifferaw et al. (2017) investigated the stability and strength of Z-purlins, taking into account cross-sectional distortions induced by wind uplift. They examined the collapse behavior of a trapezoidal thin-walled steel roof panel-purlin system under spatially and directionally variable wind loading. For this purpose, they developed a computational fluid dynamics model to generate refined spatially-varying wind loading and validated the model with the NIST-UWO database (NIST 2004a). For a more complete survey of research on light steel structures exposed to wind hazards, the reader is referred to Hancock (2016), Schafer (2017), and Yang and Bai (2017). Other aspects of wind loading, in particular, the calculation of peaks, are reviewed in the subsequent relevant sections.

Method

The method consists of the following four steps, which are explained in more detail in the Supplemental Data.

Step 1: Assign Wind Loads to Purlins

Roof panels are modeled as one-way slabs simply supported at the purlins. Pressure tap i measures wind velocity pressures $p_i(t)$ recorded as a time series of pressure coefficients $C_{pi}(t)$, assumed uniform over a rectangular tributary area of the roof. The variables p_i and C_{pi} are functions of time, wind direction, and location on the building enclosure.The NIST-UWO database (NIST 2004a) normalizes C_{pi} with respect to the mean hourly wind speed, V_{3600}, at a reference height. Conversion (Durst 1960, ASCE 7-16 Commentary 2017, Fig. C26.5-1) to the 3-s wind gust speed, V_3, allows the use of ASCE 7-16 (ASCE 2017) wind maps (ρ = air density). In this example calculation, $V_3 = 143.5$ mi/h $= 64.15$ m/s

$$p_i(t) = \tfrac{1}{2}\,\rho V_{3600}^2 C_{pi}(t) = \tfrac{1}{2}\,\rho\left(\frac{V_{3600}}{V_3}\right)^2 V_3^2 C_{pi}(t) = \tfrac{1}{2}\,\rho\left(\frac{1}{1.52}\right)^2 V_3^2 C_{pi}(t) \quad (1)$$

The wind load corresponding to tap i is transferred to the two closest purlins on either side of tap i and in inverse proportion to the distances between tap i and the purlins. For each of the 16 purlins and 37 wind directions in this example, summation of pressures over the entire area spanned by the purlins results in 19 load segments (force/length) corresponding to the 19 rows of pressure taps along the purlin length. As each load segment is subjected to a load time series with 50,000 entries, this step results in a load matrix $[\boldsymbol{L}] = [\mathbf{50{,}000\ rows\ 19\ columns}]$ for each purlin and each wind direction. The ASCE-7 sign convention is followed, whereby positive pressures point downward on the roof and inward on the walls.

Step 2: Moment and Shear Influence Coefficients for Unit Line Loads over Length Tributary to Pressure Cells

The next step is to calculate the requisite influence coefficients representing the bending moment or the shear force at various locations along the purlins, induced by the distributed loads in each of the 19 load segments. This structural analysis of a continuous beam can be performed by any number of commercial or proprietary software available to the building designer (ANSYS version 17.0 and MATLAB version R2018a were used in this study). For linear elastic behavior assumed in this study, the influence coefficients do not depend on the properties of the cross section, provided it is the same over the length of the purlin, as is assumed in this work in accordance with common practice. For long purlins consisting of several lengths, the connections are two nested portions joined together, with the bolts connecting the roof panels penetrating through both purlins (Soroushian and Pekoz 1982; Chung and Ho 2004; Laboube and Jaks 2008; Access Steel 2009). The joints are considered to be part of a continuous beam with the same cross section as the rest of the purlin.

The influence coefficients are output at 0, 1/4, 1/2, and 3/4 of the distance between the frame supports and at the ends of all load segments, 51 locations in total. For the 19 load segments, the influence coefficient matrices have size $[\boldsymbol{M_{inf}}] = [\mathbf{51}\quad\mathbf{19}]$ for moments and $[\boldsymbol{F_{inf}}] = [\mathbf{58}\quad\mathbf{19}]$ for shear. The shear influence coefficient matrix has more rows than the moment influence coefficient matrix because the internal supports have different values of shear on their left and their right.

Step 3: Peak Moments and Shear Forces for Nondirectional Wind Speed

In this step, the only directional effects considered are those pertaining to the aerodynamic behavior of the structure. Wind climatological effects are not taken into account. For each purlin, the time series of moment $[\boldsymbol{M}]$ and shear force $[\boldsymbol{F}]$ at the 51 locations being considered are calculated separately for each of the 37 directions for which pressure coefficients were obtained in the wind tunnel. In all cases, the 3-s wind speed is assumed to be 143.5 mi/h (64.15 m/s). The choice of this value will be explained in Step 4. The requisite calculations consist of the multiplication of the load matrix, obtained in Step 1, by the transpose (denoted by the superscript $\boldsymbol{T}$) of the respective influence coefficient matrices obtained in Step 2

$$[\boldsymbol{M}] = [\boldsymbol{L}] \times [\boldsymbol{M_{inf}}]^T \quad \text{or} \quad [\mathbf{50000}\quad\mathbf{51}] = [\mathbf{50000}\quad\mathbf{19}] \times [\mathbf{51}\quad\mathbf{19}]^T \quad (2a)$$

$$[\boldsymbol{F}] = [\boldsymbol{L}] \times [\boldsymbol{F_{inf}}]^T \quad \text{or} \quad [\mathbf{50000}\quad\mathbf{58}] = [\mathbf{50000}\quad\mathbf{19}] \times [\mathbf{58}\quad\mathbf{19}]^T \quad (2b)$$

The peaks of the time series of moment and shear are estimated by the translation method (Sadek and Simiu 2002), available on the NIST (2004a) wind website, which invokes the gamma distribution and the normal distribution to estimate the peaks corresponding, respectively, to the upper and lower tails of the time series' histograms. The peak distribution is represented by the Extreme Value Type I (Gumbel) distribution, and the value selected corresponds to the mean of this distribution applied to the upper and lower tails. This method has been used to evaluate components and cladding pressure coefficients that are consistent with ASCE 7-16 (Duthinh et al. 2018; Kopp and Morrison 2018) and Main Wind Force Resisting Systems (Main and Fritz 2006). In this study, a storm duration of 1 h is used, consistent with ASCE 7-16 (ASCE 2017), Eqs. 26.11-11 (Mooneghi et al. 2015; Simiu 2011). This translation method uses a duration ratio that relates the storm duration to the wind tunnel test duration converted to full scale [see Duthinh et al. (2018) for derivation].

Results are shown for purlins selected to span the different roof pressure zones defined in ASCE 7-16 (Fig. 1). Once the peaks in time are obtained for 51 locations on the purlins, shown in Figs. 2 and 3, peaks can be further selected in space, i.e., over locations and over wind directions. The selection of the peaks over all wind

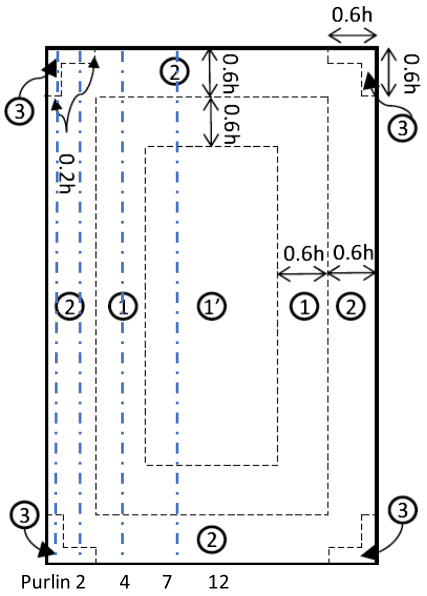

Fig. 1. Wind velocity pressure zones and purlin numbers. (Adapted from ASCE 7-16.)

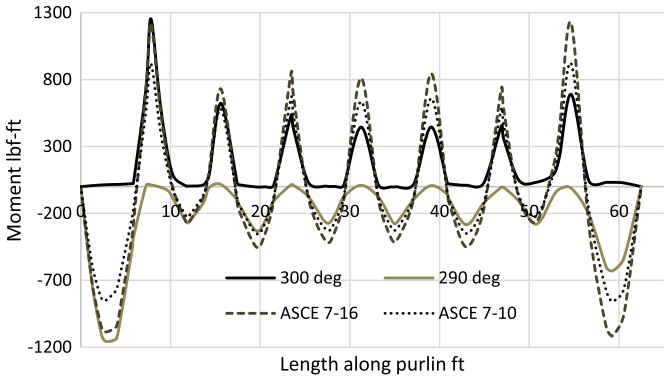

Fig. 2. Peaks of moment for purlin 2 for worst wind directions and comparison with ASCE 7-16 edge zone 2 and length of corner zone 3 and with ASCE 7-10 (1 ft = 0.3048 m; 1lbf · ft = 1.3558 N · m).

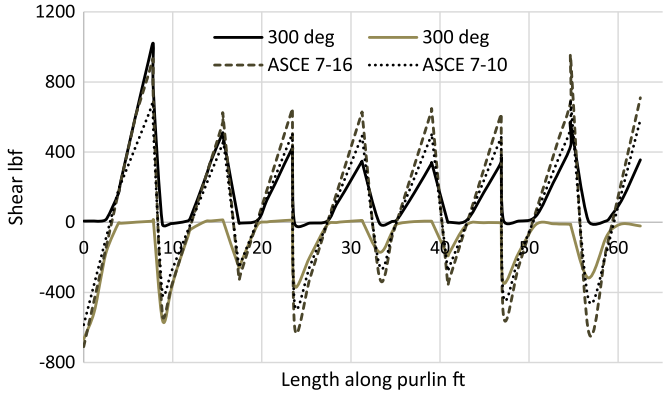

Fig. 3. Peaks of shear for purlin 2 for worst wind directions and comparison with ASCE 7-16 edge zone 2 and length of corner zone 3 and with ASCE 7-10 (1 ft = 0.3048 m; 1 lbf = 4.4482 N).

directions is inherent in the envelope method, as defined in the ASCE 7 Standard. Depending on how many different cross sections the designers want to use for the building, they can choose one overall peak or more fine-grained peaks. If a purlin has varying cross sections and some of these change in a second design iteration, it may be necessary to recalculate the influence coefficients. The final design must also account for other loads, such as snow and dead loads and ease and cost of construction.

For all 16 purlins spanning half of the roof of Building 7, results include the peaks in moment and shear extrapolated to a 1-h storm by the translation method, together with the wind direction θ_a and the location along the purlin length where the peaks occur. Some of these results are shown in the graphs in the next section. Note that wind direction θ_a refers to aerodynamic effects, i.e., the wind direction with respect to the building model in the wind tunnel, and not to climatological effects, which will be addressed in Step 4.

Nondirectional Wind Speed Results and Comparison with ASCE 7 (before Application of K_d)

ASCE 7-16 defines four zones (Fig. 1): an L-shaped corner zone 3, edge zones 2, an interior zone 1', and an intermediate zone 1 between 1' and 2 [Figs. 30.3-2A, ASCE 7-16 (ASCE 2017)], whereas ASCE 7-10 (ASCE 2010) only defines three zones. Four different purlins are used for comparison with ASCE 7-16: purlin 2 (Figs. 2 and 3) crosses edge zone 2 and the length of the corner L, and purlin 4, farther inside, crosses edge zone 2 and the width of the corner L. Purlin 12 crosses interior zone 1', intermediate zone 1, and edge zone 2; and purlin 7 crosses intermediate zone 1 and edge zone 2. In Fig. 1 or Figs. 30.3-2A [ASCE 7-16 (ASCE 2017)], the length h is taken to be the same as in the next figure, Figs. 30.3-2B [ASCE 7-16 (ASCE 2017)], where $0.4h = 10\%$ of least horizontal dimension, or $h = 10$ ft $= 3.048$ m for this low-rise building. Results for purlins 4, 7, and 12 are shown in the Supplemental Data.

Nondirectional wind speed refers in this study to the ASCE 7-16 Envelope Method in which the effects of the aerodynamically most demanding wind direction are identified. Proper comparison with database-assisted design (DAD) results precludes the use of the wind directionality factor K_d at this stage. Figs. 2 and 3 show the peaks of bending moment and shear force for purlin 2 subjected to the aerodynamically most demanding wind directions. They also show the moment and shear distribution derived from the wind velocity pressure zones specified in ASCE 7-10 and 7-16 (before the application of the wind directionality factor K_d). Because the ASCE wind pressures do not vary in time, they produce continuous moment and shear curves that are the conventional curves for a continuous beam. In contrast, the DAD results vary in time, and thus two separate curves are obtained for the maximum (positive peak) and the minimum (negative peak) over time.

For wind directions not perpendicular to the purlins, one end of a purlin is more heavily loaded than the other. It is expected that the less loaded end would be subjected to loads well below the ASCE 7 design loads, and that is indeed the case. For the more heavily loaded end, the agreement with ASCE 7-16 is good, but in four cases, the DAD highest values exceed the specifications (referenced as 100%): in Figs. 2 and 3, which involve purlin 2 over edge zone 2 and the length of corner zone 3, positive and negative moments and positive shear exceed the specifications by 3%, 3%, and 10%, respectively; and negative shear for purlin 7, which spans zones 1 and 2, exceeds specifications slightly, by 1% (Table 1). In all other cases, ASCE 7-16 envelops the highest DAD peaks quite well, sometimes exceeding the demand significantly (Table 1, positive moment for purlin 12), even though sometimes nongoverning (for purlins of uniform cross section over their length) secondary

Table 1. Positive and negative peaks of moment and shear for purlins 2, 4, 12, and 7, and for a nondirectional wind speed of 143.5 mi/h (64.15 m/s), before application of K_d

	Moment					Shear				
	ASCE 7-16 (100%)		Step 3			ASCE 7-16 (100%)		Step 3		
Purlin	lbf · ft	N · m	lbf · ft	N · m	%	lbf	N	lbf	N	%
2+	1,221	1,655	1,254	1,700	**103**	929	4,134	1,019	4,531	**110**
4+	1,051	1,424	885	1,200	84	784	3,486	690	3,069	88
12+	865	1,172	645	875	**75**	672	2,989	538	2,393	80
7+	888	1,204	701	951	79	675	3,003	571	2,542	85
2−	−1,116	−1,513	−1,147	−1,555	**103**	−710	−3,158	−667	−2,967	94
4−	−837	−1,135	−755	−1,024	90	−608	−2,703	−522	−2,320	86
12−	−813	−1,103	−751	−1,019	92	−513	−2,280	−438	−1,948	85
7−	−801	−1,085	−778	−1,055	97	−510	−2,267	−515	−2,293	**101**

Note: Unconservative values (>100%) and smallest conservative value (<100%) are in bold.

peaks fall outside of the envelope. In contrast, the ASCE 7-10 specifications result in a significant underestimation compared to the DAD results. The general good agreement with ASCE 7-16 is expected because the pressures specified in ASCE 7-16 were obtained from the same NIST-UWO data and also extrapolated to a 1-h storm duration, albeit using a different statistical process, the Best Linear Unbiased Estimator (BLUE) (Lieblein 1974) and 78% nonexceedance of the Gumbel distribution (Kopp and Morrison 2018). For a discussion of what quantile exceedance to use, the reader is referred to Simiu (2011).

Table 1 shows that ASCE 7-16 specifications exceed DAD values in most cases, as is expected of a simplified envelope method. However, as previously noted, four instances of unconservatism were found, one of which (10%) is not negligible. These exceedances reflect the approximation required to make the ASCE 7-16 pressure zones and values work safely in most cases and still be fairly simple. In contrast, the DAD method uses the wind tunnel pressure measurements directly or by interpolation and avoids this kind of discrepancy.

Step 4: Peak Moments and Shears with Specified Mean Recurrence Interval Estimated by Accounting for Wind Directionality and Building Orientation

The method proposed in this paper is illustrated by using the NIST coastal hurricane wind speed database over open terrain (NIST 2004b). The data can be transformed into wind speeds over suburban terrain by accounting for surface roughness (Simiu and Yeo 2019, § 2.3.6). Inland hurricane wind speeds are also available commercially (Simiu and Yeo 2019, § 3.2.3.2). For nonhurricane wind regions, the Standardized Extreme Wind Speed Database For The United States (NIST 2004a) can be used in lieu of the hurricane wind speed database. The wind speed data are simulated hurricane 1-min wind speeds in knots (1 knot = 0.5144 m/s) at 10 m above ground in terrain with open exposure near the US coastline (Batts et al. 1980). There are 55 files with data for locations ranging from Milepost 150 (near Port Isabel, Texas) to Milepost 2850 (near Portland, Maine), spaced at 50 nautical-mile (92.6 km) intervals. In this example calculation, Milepost 1600 on the central Florida Atlantic coast is used (Table 2). The data for each of the 999 simulated storms comprise the maximum wind speeds in 16 specified directions θ_h, beginning with North-North-East (NNE) and moving clockwise to North (N) by steps of 22.5°. The maximum wind speed for any direction is also included for each storm.

In this database, $n = 999$ is the number of hurricanes for which directional wind speed data are simulated, and the rate of hurricane occurrence is $\lambda = 0.631/\text{year}$ at Milestone 1600. According to nonparametric statistics, the mean recurrence interval (MRI) of the event that the highest wind effects in the sample will occur is $\bar{N}_1 = (n+1)/(q\lambda) = 1{,}000/(1 \times 0.631) = 1{,}585$ years for $q = 1$, where q is the order of the peak; for the second highest values, the MRI is $\bar{N}_2 = 1{,}000/(2 \times 0.631) = 792$ years for $q = 2$; for the third-highest values, the MRI is $\bar{N}_3 = 1{,}000/(3 \times 0.631) = 528$ years for $q = 3$; etc. (Simiu and Yeo 2019). For comparison with ASCE 7-16 Standard, which uses an MRI of 700 years (ASCE 7-16, p. 252), the second-highest wind speed in any direction is selected as the nondirectional wind speed for Milestone 1600. It is 101.71 knots (52.32 m/s), 1-min wind speed for storm 144, which converts to 143.5 mi/h (64.14 m/s), 3-s wind speed, and agrees with ASCE 7-16 (ASCE 2017) nondirectional wind map for Milestone 1600 (Figs. 26.5-1B, p. 253). This value was used in Step 3. (The wind speed corresponding to an MRI of 700 years could be obtained by linear interpolation between the second- and the third-highest storms. As the third-highest wind speed was very close to the second highest (Table 2), this step was omitted in this study for simplicity.)

Let θ_a be the angle between the wind direction and the axis y of the building. Wind pressure data are given in the NIST-UWO database for 37 wind directions with angle θ_a ranging from 0° to 90° and from 270° to 360° every 5°. In general, the wind direction in the building local coordinates is denoted by θ_b, where 0° and 90° correspond to the $+y$ and the $+x$ directions, respectively, and + is clockwise. For the 37 wind directions where data were

Table 2. Three highest directional wind speeds in knots (1 knot = 0.5144 m/s) for Milepost 1600, where the annual rate of hurricane occurrence is 0.631

Directions[a]																	
1	2	3	4	5	6	7	8	9	10	11	12	13	14	15	16	Max.	Storm
111.27	112.86	0	0	0	0	116.18	66.32	0	0	0	0	0	0	0	62.53	116.18	33
0	88.05	98.41	0	101.01	101.71	91.35	0	0	0	0	0	0	0	0	0	101.71	144
0	0	0	96.14	96.67	0	0	0	0	0	0	0	0	100.82	101.23	0	101.23	655

Source: Data from NIST (2004b).
[a]Every 22.5° clockwise, 1 is North-North-East and 16 is North.

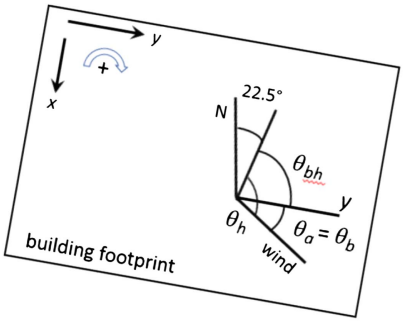

Fig. 4. Wind direction and building orientation.

collected in the wind tunnel, $\theta_b = \theta_a$ (Fig. 4). In the other directions, symmetry is invoked to relate θ_b to θ_a. The building orientation is defined by the angle θ_{bh} between the NNE (22.5° E of N) direction and the building $+y$-axis. The wind direction is defined by the angle θ_h with respect to the NNE direction. It follows from these definitions that $\theta_h - \theta_{bh} = \theta_b$. Table 3 shows how several wind tunnel directions are grouped with the same hurricane wind direction, given the lower angular resolution of the latter compared with the former.

To account for climatological effects and building orientation, and for all purlins of interest, Step 4 consists of the following substeps:

1. Select a building orientation θ_{bh}.
2. Select a wind direction θ_b.
3. From Table 3, obtain θ_a corresponding to θ_b. From Step 3, find the peak wind effects (over time and over purlin length) corresponding to θ_a and normalized to a unit wind speed.
4. From Table 3, obtain the hurricane wind direction $\theta_h = \theta_b + \theta_{bh}$. From the hurricane database, read 999 wind speeds corresponding to θ_h, and use these wind speeds squared to scale the normalized peak wind effects.
5. For each $\pm$ value of moment and shear, select the 2nd highest wind effect of these 999 storms, which corresponds to an MRI of 792 years, or interpolate linearly between the 2nd and 3rd highest wind effects for an MRI of 700 years.
6. Return to substep b and repeat for all 72 wind directions θ_b (360°/5° = 72).
7. Select the peak (over wind directions θ_b) of those 72 sets of wind effects.
8. Return to substep a and repeat for another building orientation. Substep h is unnecessary if the building orientation is already decided.

Tables 4 and 5 list the peak wind effects for purlins 2, 4, 12, and 7 and five building orientations. Due to building symmetry, these five building orientations in one quadrant suffice to fully account for directionality effects. These tables show that, by explicitly accounting for climatological effects and building orientation, the DAD method predicts peak moments that are lower by up to 25% or higher by up to 14%, and peak shear forces that are lower by up to 25% or higher by up to 21% (bold) than ASCE 7-16 (referenced as 100%), depending on building orientation. Note that in this step, wind direction is explicitly accounted for in DAD, whereas the directionality factor $K_d = 0.85$ is used for ASCE 7-16. (Compare Table 4 with Table 1, purlin 2+ moment, 1,221 lbf · ft × 0.85 = 1,038 lbf · ft or 1,655 N · m × 0.85 = 1,407 N · m.)

Conclusion

For the database-assisted design of low-rise building purlins and girts, a method is proposed that explicitly accounts for wind directionality by using directional wind tunnel measurements, directional wind speed data, and publicly available software. The method calculates peak moments and shear forces from wind tunnel pressure measurements and influence coefficients. Next, it uses a wind climatological database to account for building orientation and directionality of the wind speeds. For one example of wind effects on purlins, (1) comparison of the Envelope Method in ASCE 7-16 (taken as 100%) with the most demanding aerodynamic case from wind tunnel tests shows differences ranging between +10% and −25% (Table 1), and (2) comparison of the ASCE 7-16 method accounting for the wind directionality factor K_d with directional wind loads and using nonparametric statistical methods shows differences ranging between +21% and −25% (Tables 4 and 5). The unconservatism (+) of ASCE 7-16 is thus worse after K_d is applied. The proposed method is based on the rigorous DAD approach, accounts explicitly for the actual directional wind loading, entails no onerous computational requirements,

Table 3. Wind directions (degrees)

1st quadrant			2nd quadrant symmetrical to 1st			3rd quadrant symmetrical to 4th			4th quadrant		
θ_b	θ_a	$\theta_h - \theta_{bh}$	θ_b	θ_a	$\theta_h - \theta_{bh}$	θ_b	θ_a	$\theta_h - \theta_{bh}$	θ_b	θ_a	$\theta_h - \theta_{bh}$
5	5	0	95	85	90	185	355	180	275	275	270
10	10	0	100	80	90	190	350	180	280	280	270
15	15	22.5	105	75	112.5	195	345	202.5	285	285	292.5
20	20	22.5	110	70	112.5	200	340	202.5	290	290	292.5
25	25	22.5	115	65	112.5	205	335	202.5	295	295	292.5
30	30	22.5	120	60	112.5	210	330	202.5	300	300	292.5
35	35	45	125	55	135	215	325	225	305	305	315
40	40	45	130	50	135	220	320	225	310	310	315
45	45	45	135	45	135	225	315	225	315	315	315
50	50	45	140	40	135	230	310	225	320	320	315
55	55	45	145	35	135	235	305	225	325	325	315
60	60	67.5	150	30	157.5	240	300	247.5	330	330	337.5
65	65	67.5	155	25	157.5	245	295	247.5	335	335	337.5
70	70	67.5	160	20	157.5	250	290	247.5	340	340	337.5
75	75	67.5	165	15	157.5	255	285	247.5	345	345	337.5
80	80	90	170	10	180	260	280	270	350	350	360
85	85	90	175	5	180	265	275	270	355	355	360
90	90	90	180	360	180	270	270	270	360	360	360

Table 4. Directional peaks for ± moments for purlins 2, 4, 12, and 7, five building orientations, and a 3-s wind speed of 143.5 mi/h or 64.15 m/s; ASCE 7-16 values use $K_d = 0.85$

	Purlin 2			Purlin 4			Purlin 12			Purlin 7		
θ_{bh}°	lbf · ft	N · m	%	lbf · ft	N · m	%	lbf · ft	N · m	%	lbf · ft	N · m	%
DAD (+)												
0	1,006	1,364	97	682	924	76	560	759	76	564	765	**75**
22.5	1,099	1,490	106	693	939	78	574	778	78	633	858	84
45	965	1,308	93	732	992	82	603	817	82	631	856	84
67.5	1,179	1,598	**114**	742	1,006	83	626	848	85	679	921	90
90	1,147	1,555	111	774	1,050	87	577	782	78	596	809	79
ASCE 7-16 (+)	1,038	1,407	100	893	1,211	100	735	996	100	755	1,023	100
DAD (−)												
0	−914	−1,239	96	−606	−821	85	−615	−833	89	−618	−837	91
22.5	−1,009	−1,368	106	−594	−805	83	−605	−821	88	−606	−821	89
45	−896	−1,215	94	−669	−907	94	−549	−745	79	−651	−883	96
67.5	−1,083	−1,468	**114**	−677	−918	95	−634	−860	92	−690	−936	101
90	−1,041	−1,412	110	−611	−829	86	−676	−917	98	−669	−907	98
ASCE 7-16 (−)	−949	−1,286	100	−712	−965	100	−691	−937	100	−680	−923	100

Note: Unconservative values (>100%) and smallest conservative value (<100%) are in bold.

Table 5. Directional peaks for ± shear for purlins 2, 4, 12, and 7, five building orientations, and a 3-s wind speed of 143.5 mi/h or 64.15 m/s; ASCE 7-16 values use $K_d = 0.85$

	Purlin 2			Purlin 4			Purlin 12			Purlin 7		
θ_{bh}°	lbf	N	%	lbf	N	%	lbf	N	%	lbf	N	%
DAD (+)												
0	833	3,708	106	527	2,343	79	440	1,955	77	471	2,097	82
22.5	889	3,953	112	628	2,795	94	431	1,917	**75**	523	2,326	91
45	776	3,450	98	562	2,500	84	461	2,051	81	520	2,311	91
67.5	953	4,241	**121**	674	2,999	101	491	2,185	86	561	2,496	98
90	950	4,225	120	600	2,671	90	471	2,094	82	478	2,126	83
ASCE 7-16 (+)	790	3,514	100	666	2,963	100	571	2,541	100	574	2,552	100
DAD (−)												
0	−583	−2,594	97	−448	−1,995	87	−362	−1,609	83	−410	−1,825	95
22.5	−595	−2,645	99	−451	−2,005	87	−369	−1,641	85	−426	−1,894	98
45	−510	−2,269	85	−460	−2,048	89	−349	−1,551	80	−409	−1,819	94
67.5	−612	−2,723	101	−501	−2,229	97	−378	−1,680	87	−458	−2,039	106
90	−665	−2,956	110	−441	−1,961	85	−412	−1,834	95	−452	−2,010	104
ASCE 7-16 (−)	−603	−2,684	100	−517	−2,298	100	−436	−1,938	100	−433	−1,927	100

Note: Unconservative values (>100%) and smallest conservative value (<100%) are in bold.

and typically results in more economical designs while assuring risk-consistent safety.

Disclaimer

1. The policy of the National Institute of Standards and Technology is to use the International System of Units (SI) in its technical communications. However, in this technical note, building codes and standards are referenced in both customary (as is the practice in the US construction industry) and SI units.
2. Some commercial products are identified in this technical note for the traceability of results. Such identification does not imply recommendation or endorsement by the National Institute of Standards and Technology, nor does it imply that the products identified are necessarily the best available for the purpose.

Supplemental Data

Tables S1 and S2, and Figs. S1–S30 are available online in the ASCE Library (www.ascelibrary.org).

References

Access Steel. 2009. "Scheme development: Purlin structure design." Accessed March 20, 2018. http://www.fire-research.group.shef.ac.uk/portals/Files/Purlins/Purlin%20structure%20design.pdf.

ASCE. 2010. *Minimum design loads for buildings and other structures*. ASCE 7. Reston, VA: ASCE.

ASCE. 2017. *Minimum design loads for buildings and other structures*. ASCE 7-16. Reston, VA: ASCE.

Batts, M. E., E. Simiu, and L. R. Russell. 1980. "Hurricane wind speeds in the United States." *J. Struct. Div.* 106 (ST10): 2001–2016.

Chung, K. F., and H. C. Ho. 2004. "Structural behaviour of high strength cold-formed steel Z-purlins with overlaps." In Vol. 6 of *Proc., 17th Int. Specialty Conf. on Cold-Formed Steel Structures*. Orlando, FL.

Durst, C. S. 1960. "Wind speeds over short periods of time." *Meteor. Mag.* 89 (1056): 181–187.

Duthinh, D., J. A. Main, M. L. Gierson, and B. M. Phillips. 2018. "Analysis of wind pressure data on components and cladding of low-rise buildings." *J. Risk Uncertainty Eng. Syst. Part A: Civ. Eng.* 4 (1): 04017032. https://doi.org/10.1061/AJRUA6.0000936.

Hancock, G. J. 2016. "Cold-formed steel structures: Research review 2013–2014." *Adv. Struct. Eng.* 19 (3): 393–408. https://doi.org/10.1177/1369433216630145.

Ho, T. C. E., D. Surry, and D. Morrish. 2003a. "NIST/TTU cooperative agreement—Windstorm mitigation initiative: Wind tunnel experiments on generic low buildings." Accessed February 15, 2019. https://www.nist.gov/sites/default/files/documents/2017/08/03/blwt-ss20-2003.pdf.

Ho, T. C. E., D. Surry, and M. Nywening. 2003b. "NIST/TTU cooperative agreement—Windstorm mitigation initiative: Further experiments on generic low buildings." Accessed February 15, 2019. https://www.nist.gov/sites/default/files/documents/2017/08/03/blwt-ss21-2003.pdf.

Jayasinghe, N. C., J. D. Ginger, D. J. Henderson, and G. R. Walker. 2018. "Distribution of wind loads in metal-clad roofing structures." *J. Struct. Eng.* 144 (4): 04018014. https://doi.org/10.1061/(ASCE)ST.1943-541X.0001992.

Kopp, G. A., and M. J. Morrison. 2018. "Component and cladding wind loads for low-slope roofs on low-rise buildings." *J. Struct. Eng.* 144 (4): 04018019. https://doi.org/10.1061/(ASCE)ST.1943-541X.0001989.

Laboube, R. A., and B. Jaks. 2008. "Using cold-formed steel members: Where do I begin?" Structure Magazine. Accessed August 2008. https://www.structuremag.org/wp-content/uploads/2014/08/C-StuctralPractices-Laboube-Aug081.pdf.

Lieblein, J. 1974. *Efficient methods for extreme-value methodology.* Rep. No. NBSIR 74-602. Gaithersburg, MD: National Institute of Standards and Technology.

Main, J., and W. P. Fritz. 2006. *Database-assisted design for wind: Concepts, software, and examples for rigid and flexible buildings*. NIST Building Science Series 180. Gaithersburg, MD: National Institute of Standards and Technology.

Mooneghi, A. M., P. A. Irwin, and A. G. Chowdhury. 2015. "Partial turbulence simulation method for small structures." In *Proc., 14th Int. Conf. on Wind Engineering*. Kanagawa, Japan: Tokyo Polytechnic Univ.

NIST. 2004a. "Extreme winds and wind effects on structures." Accessed March 4, 2018. https://www.itl.nist.gov/div898/winds/homepage.htm.

NIST. 2004b. "Extreme winds and wind effects on structures." Accessed March 4, 2018. https://www.itl.nist.gov/div898/winds/hurricane.htm.

Sadek, F., and E. Simiu. 2002. "Peak non-Gaussian wind effects for database-assisted low-rise building design." *J. Eng. Mech.* 128 (5): 530–539. https://doi.org/10.1061/(ASCE)0733-9399(2002)128:5(530).

Schafer, B. W. 2017. "Developments in research and assessment of steel structures: highlights from the perspective of an American researcher." In *Proc., Eurosteel 2017*. Copenhagen, Denmark: Technical Univ. of Denmark.

Shifferaw, Y., K. Woldeyes, and G. Bitsuamlak. 2017. "Stability and strength behavior of thin-walled roof-panel-purlin system under wind loading." In *Proc., Annual Stability Conf. Structural Stability Research Council*, 650–668. Chicago: Structural Stability Research Council.

Simiu, E. 2011. *Design of buildings for wind*. 2nd ed. Hoboken, NJ: Wiley.

Simiu, E., and D. Yeo. 2019. *Wind effects on structures: Modern structural design for wind*. 4th ed. New York: Wiley.

Soroushian, P., and T. Pekoz. 1982. "Behavior of C- and Z-purlins under wind uplift." In *Proc., 6th Int. Specialty Conf. on cold-formed steel structures*. Rolla, MO: Missouri Univ. of Science and Technology.

Tamura, Y. 2012. "Aerodynamic database for low-rise buildings." Accessed September 1, 2018. http://www.wind.arch.t-kougei.ac.jp/info_center/windpressure/lowrise/mainpage.html.

Yang, N., and F. M. Bai. 2017. "Damage analysis and evaluation of light steel structures exposed to wind hazards." *Appl. Sci.* 7 (3): 239. https://doi.org/10.3390/app7030239.